J. Fluid Mech. (2012), *vol.* 701, *pp.* 278–303.
doi:10.1017/jfm.2012.158

Turbulent buoyant convection from a maintained source of buoyancy in a narrow vertical tank

Daan D. J. A. van Sommeren[1,2], C. P. Caulfield[1,2]† and Andrew W. Woods[1]

[1] BP Institute, University of Cambridge, Madingley Road, Cambridge CB3 0EZ, UK

[2] Department of Applied Mathematics and Theoretical Physics, University of Cambridge, Centre for Mathematical Sciences, Wilberforce Road, Cambridge CB3 0WA, UK

(Received 21 August 2011; revised 6 February 2012; accepted 27 March 2012; first published online 10 May 2012)

We describe new experiments to examine the buoyancy-induced mixing which results from the injection of a small constant volume flux of fluid of density ρ_s at the top of a long narrow vertical tank with square cross-section which is filled with fluid of density $\rho_0 < \rho_s$. The injected fluid vigorously mixes with the less dense fluid which initially occupies the tank, such that a dense mixed region of turbulent fluid propagates downwards during the initial mixing phase of the experiment. For an ideal source of constant buoyancy flux B_s, we show that the height of the mixed region grows as $h \sim B_s^{1/6} d^{1/3} t^{1/2}$ and that the horizontally averaged reduced gravity $\overline{g'} = g(\overline{\rho} - \rho_0)/\rho_0$ at the top of tank increases as $\overline{g'}(0) \sim B_s^{5/6} d^{-7/3} t^{1/2}$, where d is the width of the tank. Once the mixed region reaches the bottom of the tank, the turbulent mixing continues in an intermediate mixing phase, and we demonstrate that the reduced gravity at each height increases approximately linearly with time. This suggests that the buoyancy flux is uniformly distributed over the full height of the tank. The overall density gradient between the top and bottom of the mixed region is hence time-independent for both the mixing phases before and after the mixed region has reached the bottom of the tank. Our results are consistent with previous models developed for the mixing of an unstable density gradient in a confined geometry, based on Prandtl's mixing length theory, which suggest that the turbulent diffusion coefficient and the magnitude of the local turbulent flux are given by the nonlinear relations $\kappa_T^{nl} = \lambda^2 d^2 \left(\partial \overline{g'}/\partial z\right)^{1/2}$ and $J^{nl} = \lambda^2 d^2 \left(\partial \overline{g'}/\partial z\right)^{3/2}$, respectively. The $O(1)$ constant λ relates the width of the tank to the characteristic mixing length of the turbulent eddies. Since the mixed region is characterized by a time-independent overall density gradient, we also tested the predictions based on a linear model in which the turbulent diffusion coefficient is approximated by a constant κ_T^l. We solve the corresponding nonlinear and linear turbulent diffusion equations for both mixing phases, and show a good agreement with experimental profiles measured by a dye attenuation technique, in particular for the solutions based on the nonlinear model.

Key words: mixing and dispersion, turbulent convection, turbulent mixing

† Email address for correspondence: cpc12@cam.ac.uk

1. Introduction

Buoyancy-induced turbulent mixing is a fundamental process in many industrial and geophysical flows. Of course, we can distinguish such flows by the extent of spatial inhomogeneity in the initial or boundary conditions. Two classical archetypes that involve homogeneous initial or boundary conditions are Rayleigh–Taylor instability and Rayleigh–Bénard convection (see, for example, Dimonte *et al.* 2004; Ahlers, Grossmann & Lohse 2009, respectively). Rayleigh–Taylor instability is driven by an unstable density difference between two layers of fluid, while Rayleigh–Bénard convection is driven by a statically unstable temperature, and hence density contrast imposed on a single layer of fluid. In both cases, the redistribution of buoyancy scales with the density or imposed temperature contrast. In finite geometries, the flux also depends on the geometry and aspect ratio of the enclosed box, as studied by Dalziel *et al.* (2008) and Weiss & Ahlers (2011).

In the other extreme of strong inhomogeneity in the initial or boundary conditions, continuous releases of fluid of different density from an isolated 'source' in an enclosed space lead to the rise of a turbulent 'plume' entraining and mixing with the ambient fluid. The behaviour of such plumes is important for a number of industrial and environmental applications, as recently discussed by Woods (2010). In the limit where the cross-sectional area of a plume is negligible compared with the cross-sectional area of the enclosing box, the plume sets up and couples with a developing ambient stratification, as first investigated by Baines & Turner (1969). However, when the cross-sectional area of the plume is similar to that of the enclosing box, the plume dynamics change. Our work focuses on understanding the mixing produced by an ideal source of buoyancy with zero volume flux released into a long vertical enclosure of small cross-sectional area. This is relevant for flows in chemical reaction columns (Thakore & Bhatt 2007), magma flows in confined geophysical geometries (Ryan 1994) and heat or gas flows in mine shafts (Karmis 2001).

We report on a series of new image-analysis experiments in a narrow vertical tank with a source of constant buoyancy flux B_s at the top. The related source fluid vigorously mixes with the less dense fluid that initially occupies the tank, such that a dense mixed region of turbulent fluid propagates downwards. We focus on the turbulent flow before and after the mixed region has reached the bottom of the tank. In analysing our experiments, and in particular in developing a quantitative model of the evolving density gradient in the mixed region, we draw from a number of laboratory studies on vertical buoyancy-driven mixing in a long tank with small cross-sectional area (Barnett 1991; Holmes, Karr & Baird 1991; Baird *et al.* 1992; Zukoski 1995; Debacq *et al.* 2001; Dalziel *et al.* 2008). In these studies, the turbulent mixing is modelled as a diffusive process, although different expressions for the turbulent diffusion coefficient were adopted.

Barnett (1991) analysed the flow and density field produced by the buoyant convection from a localized plume source (Morton, Taylor & Turner 1956) in a narrow vertical tank. In particular, he considered in detail the evolution from a region dominated by plume-like dynamics towards a region dominated by turbulent convection across the whole width of the tank. Barnett (1991) modelled the evolution of the horizontally averaged density in the region dominated by turbulent convection, with a turbulent diffusion coefficient expanded in terms of integer powers of the density gradient. However, he argued that higher-order terms are negligible for the considered range of experiments, and so he approximated the turbulent diffusion coefficient by a constant value. Barnett (1991) successfully tested the predictions based on this linear model with a constant turbulent diffusion coefficient, although

Holmes *et al.* (1991) discussed experimental results which actually suggested that the turbulent diffusion coefficient should depend on the square root of the local density gradient. An empirical relation for the turbulent diffusion coefficient was derived, which was later used by Baird *et al.* (1992) to model the horizontally averaged density evolution in their experiments. Eventually, Zukoski (1995) suggested that the turbulent diffusion coefficient is given by the product of a local velocity fluctuation and a mixing length. With this, he found that the turbulent diffusion coefficient is indeed predicted to be proportional to the square root of the local density gradient, which is similar to the empirical relation found by Holmes *et al.* (1991).

In this paper, we follow Holmes *et al.* (1991), Baird *et al.* (1992) and Zukoski (1995), and apply Prandtl's mixing length theory to show that the turbulent diffusion coefficient depends on the square root of the local density gradient. By applying Prandtl's mixing length theory, the turbulent diffusion coefficient κ_T can be written as

$$\kappa_T = u_T l_T, \tag{1.1}$$

with l_T the characteristic mixing length of the turbulent eddies, and u_T the corresponding characteristic buoyancy-driven speed given by

$$u_T = l_T \sqrt{\frac{\partial \overline{g'}}{\partial z}} \sim \sqrt{\Delta \overline{g'} l_T}, \tag{1.2}$$

where the overline denotes a horizontal average of the reduced gravity $g' = g(\rho - \rho_0)/\rho_0$ across the width of the tank, g is the acceleration due to gravity, and ρ_0 is an appropriate reference density. The magnitude of the associated nonlinear turbulent flux of reduced gravity is thus given by

$$J = \kappa_T \frac{\partial \overline{g'}}{\partial z} = l_T^2 \left(\frac{\partial \overline{g'}}{\partial z} \right)^{3/2}, \tag{1.3}$$

which, alternatively, may be understood in terms of the characteristic difference in reduced gravity

$$\Delta \overline{g'} \sim l_T \left(\frac{\partial \overline{g'}}{\partial z} \right), \tag{1.4}$$

which is transported with speed u_T, such that $J \sim \Delta \overline{g'} u_T$. In a confined geometry, the characteristic mixing length l_T may be related to the width of the tank d, by an empirical $O(1)$ constant $l_T = \lambda d$, such that (1.1) and (1.3) become

$$\kappa_T^{nl} = \lambda^2 d^2 \left(\frac{\partial \overline{g'}}{\partial z} \right)^{1/2} \rightarrow J^{nl} = \lambda^2 d^2 \left(\frac{\partial \overline{g'}}{\partial z} \right)^{3/2}, \tag{1.5}$$

where we have used the superscript *nl* to denote the nonlinear form of the turbulent diffusion coefficient and the local turbulent flux. (In § 5, following the modelling approach used in Barnett (1991), we discuss a model in which the turbulent diffusion coefficient is a constant, the flux is a linear function of the reduced gravity, and so the reduced gravity satisfies a linear diffusion equation, and compare both the nonlinear model and this linear model with our experimental measurements.) From (1.5), we deduce that the nonlinear differential equation for the evolution of the reduced gravity

is given by

$$\frac{\partial \overline{g'}^{nl}}{\partial t} = \lambda^2 d^2 \frac{\partial}{\partial z}\left[\left(\frac{\partial \overline{g'}^{nl}}{\partial z}\right)^{3/2}\right], \tag{1.6}$$

in which we denote the solution of the nonlinear turbulent diffusion equation by $\overline{g'}^{nl}$.

Baird *et al.* (1992) and later Zukoski (1995) successfully tested the predictions of a model based on (1.5) with some turbulent exchange flow experiments in a long narrow vertical tank connected to a reservoir. In particular, Baird *et al.* (1992) analysed finite source release experiments and found that λ is close to one, but slightly varied with the width of the tank and the viscosity of the fluid. This observed dependence strongly suggests that λ is actually dependent on the Reynolds number, and furthermore that the actual value of λ decreases towards one with increasing Reynolds number. Dalziel *et al.* (2008) performed experiments with an image processing technique to study the turbulent mixing in a long narrow vertical tank, of width d, in which the lower half is initially filled with a clear fluid which is less dense than the dyed fluid in the upper half of the tank, with a buoyancy contrast g'. Using particle image velocimetry (PIV), they confirmed that the turbulent eddies indeed scale with the width of the tank such that λ is an $O(1)$ constant. Using calibrated light intensity as a proxy for the line-of-sight averaged density, they measured the evolving density as a function of the height and showed that a mixed region develops whose height grows as $h \sim g'^{1/5} d^{4/5} t^{2/5}$, which is consistent with (1.6).

In the present experiments, we expect the mixing to be controlled by the constant buoyancy flux B_s and the width of the tank d. As the dense mixed region of turbulent fluid deepens, there is no independent length scale controlling the extent of the mixed region, which suggests that the mixing may be self-similar. However, the flux law (1.5) suggests that the turbulent flux at the top of the tank depends on the gradient of the reduced gravity. Therefore, from dimensional analysis, we expect that the height of the mixed region h should increase as

$$h \sim B_s^{1/6} d^{1/3} t^{1/2} = h_T, \tag{1.7}$$

and that the reduced gravity at the top of the tank should grow as

$$\overline{g'}(0) \sim B_s^{5/6} d^{-7/3} t^{1/2} = \overline{g'}_T(0). \tag{1.8}$$

This ensures that the overall gradient of the reduced gravity between the top and bottom of the mixed region is time-independent, and that the total amount of buoyancy is conserved. It follows that the arrival time t_A of the mixed region at the bottom of the tank with height H has a characteristic scale t_{AA}, which depends on B, d and H according to (1.7):

$$t_A \sim H^2 B_s^{-1/3} d^{-2/3} = t_{AA}. \tag{1.9}$$

The constant buoyancy flux continues after the mixed region has reached the bottom of the tank, and we expect that the density gradient will then adjust so that the buoyancy flux becomes uniformly distributed over the full height of the tank with the density at each height increasing linearly with time.

To test this picture of the flow evolution, the paper is organized as follows. In § 2, we describe the experimental technique and discuss observations of the turbulent flow before and after the mixed region has reached the bottom of the tank. In § 3, we confirm the new scaling laws (1.7) and (1.8), and solve the nonlinear differential

equation (1.6) to predict the horizontally averaged reduced gravity distribution during this 'initial mixing phase', which we successfully compare with experimental results. The end of this initial mixing phase is defined by an effective arrival time of the mixed region at the bottom of the tank, $t_{EA} \sim t_{AA}$, deduced from experimental results, and is shown to be in good agreement with our model. We then focus on the evolution of the mixed region after it has reached the bottom of the tank in § 4. For this 'intermediate mixing phase', we demonstrate that the reduced gravity at every height increases approximately linearly with time, and that the constant buoyancy flux is thus essentially uniformly distributed over the full height of the tank. We solve the nonlinear differential equation (1.6), and we show again a good agreement with experimental results. In § 5, we discuss a linear model in which the turbulent diffusion equation is approximated by a constant, following Barnett (1991). We compare solutions based on this linear model with the nonlinear model discussed above, as well as with experimental data for both the initial and intermediate mixing phase. In § 6, we identify the limits of validity of our modelling assumptions, in which the source conditions are of particular interest. We consider the somewhat plume-like flow in the region near the source, and we examine the significance of our source with a finite volume flux and a finite density difference between the source fluid and the fluid initially in the experimental tank. Finally, in § 7, we discuss our conclusions, and briefly mention some applications of our results.

2. Experiments

2.1. *Experimental procedure*

We perform experiments in a narrow vertical tank with dimensions $d \times d \times 40d$ with $d = 5.0 \times 10^{-2}$ m. Initially, we fill the tank with fresh clear water, of density ρ_0, and a peristaltic pump then provides a constant flux Q_s of dyed salty water of density $\rho_s > \rho_0$ and reduced gravity $g'_s = g(\rho_s - \rho_0)/\rho_0 > 0$, at the top of the tank. A fine mesh is positioned close to the fluid level, such that the dyed salty water drips into the fresh clear water at random positions across the cross-sectional area of the tank with minimal momentum. In all of our experiments, the characteristic dripping frequency is high enough to approximate a continuous flux of dense fluid which is evenly distributed over the area of the tank. To conserve volume, we extract an equivalent volume flux Q_s from the bottom of the tank at $z = -H = -40d$. As discussed in § 6, this volume flux is sufficiently small so that the turbulent mixing is dominantly driven by the buoyancy flux given by

$$B_s = g'_s Q_s. \tag{2.1}$$

We define a coordinate system with the origin at the top, left front corner of the tank, as shown in figure 1(*a*). The bottom of the tank is thus at $z = -40d$, the lateral width extends $0 \leqslant x \leqslant d$, and the line-of-sight width of the tank extends $0 \leqslant y \leqslant d$. In general, the density distribution in the tank $\rho_0 \leqslant \rho(x, y, z, t) \leqslant \rho_s$.

We attach Electroluminescent LightTape (Electro-LuminX Lighting Corp.) to the rear of the tank, which provides highly uniform illumination of cyan hue. We take photographs every five seconds with a computer-controlled Nikon D90 RGB DSLR-camera at distance $100d$ from the front of the tank. The shutter speed is 1/15 s and we use ISO 800 to take images with a 52 mm (f7.1) lens. This provides a fast shutter speed to approximate an instantaneous capture of the flow dynamics, while maintaining a broad range of light intensities which the camera can capture to distinguish between different clear/dyed fluid mixtures. The experimental tank

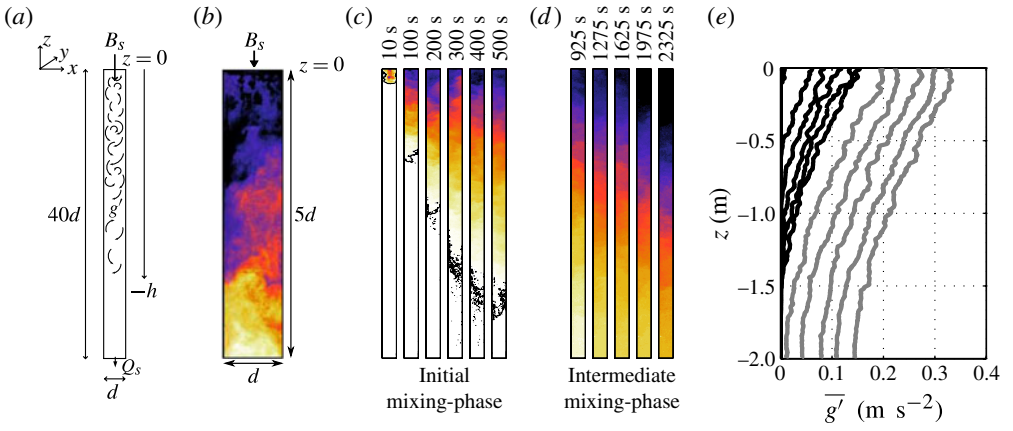

FIGURE 1. (Colour online available at journals.cambridge.org/flm) (*a*) Schematic overview of the buoyancy-induced turbulent mixing due to the injection of a small constant volume flux Q_s of dense fluid with reduced gravity g'_s at the top of a narrow vertical tank which has dimensions $d \times d \times 40d$. To maintain volume, we extract an equivalent volume flux Q_s from the bottom of the tank at $z = -40d$. As discussed in § 6, this volume flux is sufficiently small so that the turbulent mixing is dominantly driven by the source buoyancy flux $B_s = g'_s Q_s$. (*b*) A close-up image of the region near the source $-5d \leqslant z \leqslant 0$, in which the colours and the contrast are adjusted to visualize the turbulent eddies clearly, showing that they typically grow to size d within a distance $O(5d)$ from the source at $z = 0$. (*c*) Evolution of the line-of-sight averaged reduced gravity distribution $\langle g' \rangle_y(x, z, t)$ from an experiment with $B_s = 5.1 \times 10^{-7}$ m^4 s^{-3} in the initial mixing phase before the dense mixed region of turbulent fluid has reached the bottom of the tank. On each figure, we show a black contour line where $\langle g' \rangle_y = 7.5 \times 10^{-4}$ m s^{-2}, which is just above the experimental noise level. (*d*) The evolution of the mixed region after it has reached the bottom of the tank in the intermediate mixing phase, again for an experiment with $B_s = 5.1 \times 10^{-7}$ m^4 s^{-3}. (*e*) The horizontally averaged reduced gravity profiles $\overline{g'}(z, t)$ for the initial mixing phase (black lines) at the times shown in (*c*) and for the intermediate mixing phase (grey lines) at the times shown in (*d*).

occupies a region of the image of 70×3000 pixels. We perform the experiments in a dark room, whilst ensuring that the only light detected by the camera passes through the fluid in the tank. Since the source fluid of density ρ_s is coloured with red food dye (a 'Preema' product) while the initial tank fluid of density ρ_0 is clear, we can infer the line-of-sight averaged density distribution $\langle \rho \rangle_y(x, z, t)$ from the attenuated light intensity of the images, as is extensively discussed by Cenedese & Dalziel (1998). Light intensity data is obtained from the green channel, since the contrast between the red source fluid and the cyan LightTape is the highest in this channel. While Cenedese & Dalziel (1998) discussed the theoretical derivation of a calibration function between light intensity and concentration of dyed fluid, due to the nonlinear response properties of our camera, we utilize a direct calibration approach. This is carried out by taking calibration images of the tank filled with 15 different mixtures of source dyed fluid and clear initial tank fluid. To maximize the accuracy of our experimental measurements, we choose the maximum concentration calibration differently for each experiment.

We then subdivide the calibration images of the tank front surface into multi-pixel cells with sides $d/35$ in the x-direction and $d/10$ in the z-direction, and we determine an average measured light intensity in every one of these cells for each of the 15

different calibration concentrations. We then determine empirically a calibration curve for each cell using a sixth-order polynomial fit through the 15 calibration points. In this way, we use a total of 35×400 calibration curves to convert the spatially and temporally evolving light intensity field into a density distribution. We compensate for temporal variation in the light intensity of the electroluminescent tape by also imaging a thin strip of electroluminescent panel down one side of the tank. During processing, we use a linear mapping to match the measured light intensity of this strip to the average emitted intensity observed in the calibration procedure, thus compensating for observed temporal variations of the emitted light intensity, which are typically less than 1.5 % in any case.

To check the calibration quantitatively, we compare the actual total amount of source fluid (due to injection at the source) in the tank with the quantity which can be inferred from the light intensity measurements before the mixed region has reached the bottom of the tank. The two values for the total amount of source fluid in the tank typically differ by less than 3 %, a deviation which we believe is mainly due to parallax effects near both ends of the experimental tank.

Provided that the source volume flux is sufficiently small, the flow may be characterized by three quantities: the tank width d; the source (specific) buoyancy flux $B_s = g_s' Q_s$; and the total tank height H after the mixed region has reached the bottom of the tank. For both mixing phases, we perform experiments with buoyancy flux $B_s = 1.0, 2.8, 5.1, 10.0$ and 14.0×10^{-7} m^4 s^{-3}. We can distinguish between an initial mixing phase (before the mixed region has reached the bottom of the tank) and an intermediate mixing phase (after the mixed region has reached the bottom of the tank during which the density in the tank is still significantly smaller than the source density). We vary the source buoyancy flux by changing Q_s while keeping the reduced gravity of the source fluid constant with $g_s' = 1.00 \pm 0.05$ m s^{-2} for the experiments in the initial mixing phase before the mixed region reached the bottom of the tank, and with $g_s' = 1.55 \pm 0.05$ m s^{-2} for the intermediate mixing phase after the mixed region has reached the bottom of the tank. To obtain the same buoyancy flux, the set of experiments with a lower reduced gravity of the source fluid g_s' involves a higher volume flux Q_s. In practice, a higher volume flux Q_s results in a higher frequency of dense fluid dripping into the tank. This then serves as a better approximation for a continuous source flux, which is preferred when the mixed region is still growing. However, a higher reduced gravity of the source g_s' is preferred once the mixed region has reached the bottom of the tank and the reduced gravity in the region starts to approach that of the source fluid. The density in the tank ultimately converges towards the density of the source fluid, which suggests that the flow dynamics eventually change and the intermediate mixing phase is hence finite in duration. In this work, we only consider the initial and intermediate mixing phase to test our model which assumes that the source is a source of finite buoyancy alone, i.e. $g_s' \to \infty$ and $Q_s \to 0$. We discuss our underlying assumptions in more detail in § 6.

2.2. *Experimental observations*

We consider the turbulent mixing driven by a buoyancy flux B_s at the top of a narrow vertical tank with lateral scale d, such that we define the appropriate characteristic Reynolds number as

$$Re_T = \frac{B_s^{1/3} d^{2/3}}{\nu}, \tag{2.2}$$

which has a value $0.6\times10^3 < Re_T < 1.6\times10^3$ for the range of parameters considered in our experiments. These Reynolds numbers are found to be high enough for turbulent mixing to dominate in both the mixing phases. This is in agreement with observations of Dalziel *et al.* (2008) in the early, turbulent stage of Rayleigh–Taylor instability experiments which had similar Reynolds numbers. Their PIV measurements showed that a given parcel of fluid moves vertically by cascading around many complex three-dimensional vortical structures with different orientations which may change in time. Indeed, the turbulent flow is dominated by eddies of the scale d of the width of the tank, which leads to extremely efficient mixing.

To compare turbulent diffusion with molecular diffusion (of the dye in particular) we give an estimate of the turbulent diffusion coefficient, i.e. κ_T, based on Prandtl's mixing length theory (1.1) and our experimental parameters B_s and d

$$\kappa_T = B_s^{1/3}\,(\lambda d)^{2/3}, \tag{2.3}$$

with λ an $O(1)$ constant. We find that this turbulent diffusion coefficient is $O(10^{-3})$ m^2 s^{-1}, which is $\sim10^6$ larger than that typically for the molecular diffusion of the dye (Lide 2001).

The turbulent eddies typically grow to the limiting size of the tank's lateral scale d, within a distance $O(5d)$ from the source at $z = 0$, as illustrated in figure 1(*b*). This means that the assumption of a single length scale, d, is not valid in the vicinity of the source and that deviations from our model are to be expected, as discussed in more detail in § 6.

With the help of the image analysis technique, it is possible to obtain the evolution of the line-of-sight averaged reduced gravity distribution $\langle g'\rangle_y(x, z, t)$. In figure 1(*c*), we show the growth of the mixed region in terms of $\langle g'\rangle_y(x, z, t)$ for an experiment with $B_s = 5.1\times10^{-7}$ m^4 s^{-3} at times $t = 10$, 100, 200, 300, 400 and 500 s where $t = 0$ s corresponds to the first release of dense fluid and hence the start of the initial mixing phase. A black contour line at $\langle g'\rangle_y = 7.5\times10^{-4}$ m s^{-2} indicates the first detectable front of the mixed region. The 'detection' arrival time of this detectable 'first front' at the bottom of the tank is $t_{DA} = 875$, 689, 578, 453, 292 s for the experiments with $B_s = 1.0$, 2.8, 5.1, 10.0 and 14.0×10^{-7} m^4 s^{-3}, respectively. Indeed, we expect that the actual, yet undetected, true first front reaches the bottom of the tank some time before this. We therefore define (in § 3) an 'effective' arrival time t_{EA} as the end of the initial mixing phase.

Although there is undoubtedly variation in the lateral cross-tank (x) direction, this occurs typically on the overturning time scale of the eddies and is associated with the turbulence. Since we are principally interested in the evolution of the flow in the z-direction, we consider the horizontally averaged reduced gravity distribution $\overline{g'}(z, t)$. Profiles of $\overline{g'}(z, t)$ for the initial mixing phase, at the times shown in figure 1(*c*), are presented in figure 1(*e*) by black lines. The standard deviation across the width of the tank is typically 2 % of the local reduced gravity, which makes it appropriate to consider the horizontally averaged reduced gravity distribution. Both the height of the mixed region h and the reduced gravity at the top of the tank $\overline{g'}(0)$ clearly increase with time.

After the 'first front' has reached the bottom of the tank, the mixed region continues to evolve in a turbulent fashion and enters the intermediate mixing phase. Figure 1(*d*) shows the evolution of $\langle g'\rangle_y(x, z, t)$ for an experiment with $B_s = 5.1\times10^{-7}$ m^4 s^{-3} and at $t = 925$, 1275, 1625, 1975 and 2325 s. In figure 1(*e*), we plot (with grey lines) profiles of $\overline{g'}(z, t)$ at times that correspond to those shown in figure 1(*d*). Since the

profiles are approximately parallel, they suggest that the density increases with time at the same rate at every height, and so the incoming density is homogeneously distributed over the entire height of the tank. Equivalently, the overall density gradient from top to bottom is approximately independent of time in the intermediate mixing phase, although as we discuss further in § 4, the actual density profile is a nonlinear function of height.

3. Initial mixing phase: growth of the mixed region

We choose to non-dimensionalize time scales using the source buoyancy flux and the tank width so that

$$\hat{t} = tB_s^{1/3}d^{-4/3}. \tag{3.1}$$

Using this scaling, the characteristic time scale for the arrival time of the mixed region at the bottom of the tank, t_{AA} as defined in (1.9), can be expressed in non-dimensional form as $\hat{t}_{AA} = (H/d)^2 = 1600$ for our tank. For the experiments with $B_s = 1.0, 2.8, 5.1, 10.0$ and 14.0×10^{-7} m^4 s^{-3} we find that the non-dimensional arrival time of the detectable 'first front' at the bottom of the tank, $\hat{t}_{DA}$, is given by

$$\hat{t}_{DA} = 228, 245, 250, 245, 226, \tag{3.2}$$

respectively. The values for $\hat{t}_{DA}$ are all very similar, suggesting the time scale is appropriate and collapses the data. The numerical value of the scaled time is smaller than the scaling $\hat{t}_{AA}$. This difference is associated with the detailed nonlinear mixing process; in § 3.2, we solve the underlying nonlinear diffusion equation (1.6) and show that the equation indeed leads to a different (and substantially smaller than $\hat{t}_{AA}$) prediction of the numerical value for the coefficient in the scaling law. Indeed, it is reasonable to suppose that the actual arrival time of dense fluid at the bottom of the tank will be somewhat smaller than the detectable 'first front' arrival time $\hat{t}_{DA}$. Therefore, we define the effective arrival time $\hat{t}_{EA} = 200$ as a good approximation for the moment that the mixed region has reached the bottom of the tank, and thus define $0 \leqslant \hat{t} \leqslant \hat{t}_{EA} = 200$ as the time interval of the initial mixing phase. We show that this assumption is consistent with the solution of the nonlinear diffusion equation (1.6).

To test the scaling for the increasing height of the mixed region h and the reduced gravity at the top of the tank $\overline{g'}(0)$ as given by (1.7)–(1.8) in the initial mixing phase, we define the following non-dimensional quantities:

$$\eta = \frac{z}{h_T} = B_s{}^{-1/6}d^{-1/3}\left(\frac{z}{t^{1/2}}\right); \quad f = \frac{\overline{g'}}{\overline{g'}_T(0)} = B_s{}^{-5/6}d^{7/3}\left(\frac{\overline{g'}}{t^{1/2}}\right); \tag{3.3}$$

in which h_T and $\overline{g'}_T(0)$ represent the proposed scalings for the height of the mixed region, and the reduced gravity at the top of the tank, as defined by (1.7)–(1.8), respectively. In (3.3), we define η as the natural similarity variable, and f as a non-dimensional reduced gravity. Profiles of the dimensional reduced gravity are hence given by

$$\overline{g'}(z, t) = B_s{}^{5/6}d^{-7/3}t^{1/2}f(\eta). \tag{3.4}$$

3.1. *Scaling comparison*

If the hypothesized scalings for the height of the mixed region given by (1.7) and the reduced gravity at the top of the tank given by (1.8) are correct, profiles of $f(\eta)$ should be independent of time, the buoyancy flux and the width of the tank. However,

the necessary accurate measurements of h and $\overline{g'}$ required to compare our theoretical scaling predictions with experiments are difficult due to a combination of factors, including experimental noise, turbulence intermittency and the growth of turbulent eddies near the source. Therefore, we consider the integral-based first moment of the reduced gravity as defined by

$$\frac{\displaystyle\int_{-H}^{0} \overline{g'} z \,\mathrm{d}z}{\displaystyle\int_{-H}^{0} \overline{g'} \,\mathrm{d}z} = z_m \sim B_s^{1/6} d^{-1/3} t^{1/2} \leftrightarrow \frac{\displaystyle\int_{-\eta_H}^{0} f\eta \,\mathrm{d}\eta}{\displaystyle\int_{-\eta_H}^{0} f \,\mathrm{d}\eta} = \eta_m, \quad \eta_H = \frac{H}{h_T}, \tag{3.5}$$

and the standard deviation around the first moment given by

$$\sqrt{\frac{\displaystyle\int_{-H}^{0} \overline{g'} (z - z_m)^2 \,\mathrm{d}z}{\displaystyle\int_{-H}^{0} \overline{g'} \,\mathrm{d}z}} = z_{std} \sim B_s^{1/6} d^{-1/3} t^{1/2} \leftrightarrow \sqrt{\frac{\displaystyle\int_{-\eta_H}^{0} f\,(\eta - \eta_m)^2 \,\mathrm{d}\eta}{\displaystyle\int_{-\eta_H}^{0} f \,\mathrm{d}\eta}} = \eta_{std}. \tag{3.6}$$

Our scalings predict that both η_m and η_{std} are constant. Figure 2(*a*,*b*) show the evolution of both these quantities throughout the initial mixing phase, where the non-dimensional time $\hat{t}$ is defined by (3.1). We find that η_m and η_{std} fluctuate around a constant which is approximately the same for all experiments, and that the scattering decreases with time as the mixed region evolves. Table 1 shows the values of η_m, the corresponding $f_m = f(\eta_m)$, and η_{std} which are determined by time-averaging over the interval of the initial mixing phase $0 \leqslant \hat{t} \leqslant \hat{t}_{EA} = 200$. Since η_m, f_m and η_{std} only vary slightly, we believe that the scalings (1.7)–(1.8) are valid.

3.2. *Solution of the nonlinear diffusion equation*

Given the good agreement between the experimental results and the scalings (1.7)–(1.8), we substitute the non-dimensional quantities of (3.3) in the nonlinear turbulent diffusion equation (1.6), such that we find

$$f^{nl} - \eta \frac{\partial f^{nl}}{\partial \eta} = 2\lambda^2 \frac{\partial}{\partial \eta} \left[\left(\frac{\partial f^{nl}}{\partial \eta} \right)^{3/2} \right], \tag{3.7}$$

where we denote f^{nl} as the solution of this nonlinear differential equation. To solve (3.7), we impose two natural conditions. The first follows from the constant buoyancy flux located at $z = 0$, which requires the (boundary) condition (in dimensional and non-dimensional form, respectively):

$$d^2 J^{nl}|_{z=0} = \lambda^2 d^4 \left(\frac{\partial \overline{g'}^{nl}}{\partial z} \right)^{3/2} \Bigg|_{z=0} = B_s \leftrightarrow \left. \frac{\partial f^{nl}}{\partial \eta} \right|_{\eta=0} = \frac{1}{\lambda^{4/3}}. \tag{3.8}$$

The second (global integral) condition follows from the conservation of the total buoyancy in the entire tank of height H (with H large enough to assume $H \to \infty$)

$$d^2 \int_{-H}^{0} \overline{g'}^{nl} \,\mathrm{d}z = B_s t \leftrightarrow \int_{-\eta_H}^{0} f^{nl} \,\mathrm{d}\eta = 1, \tag{3.9}$$

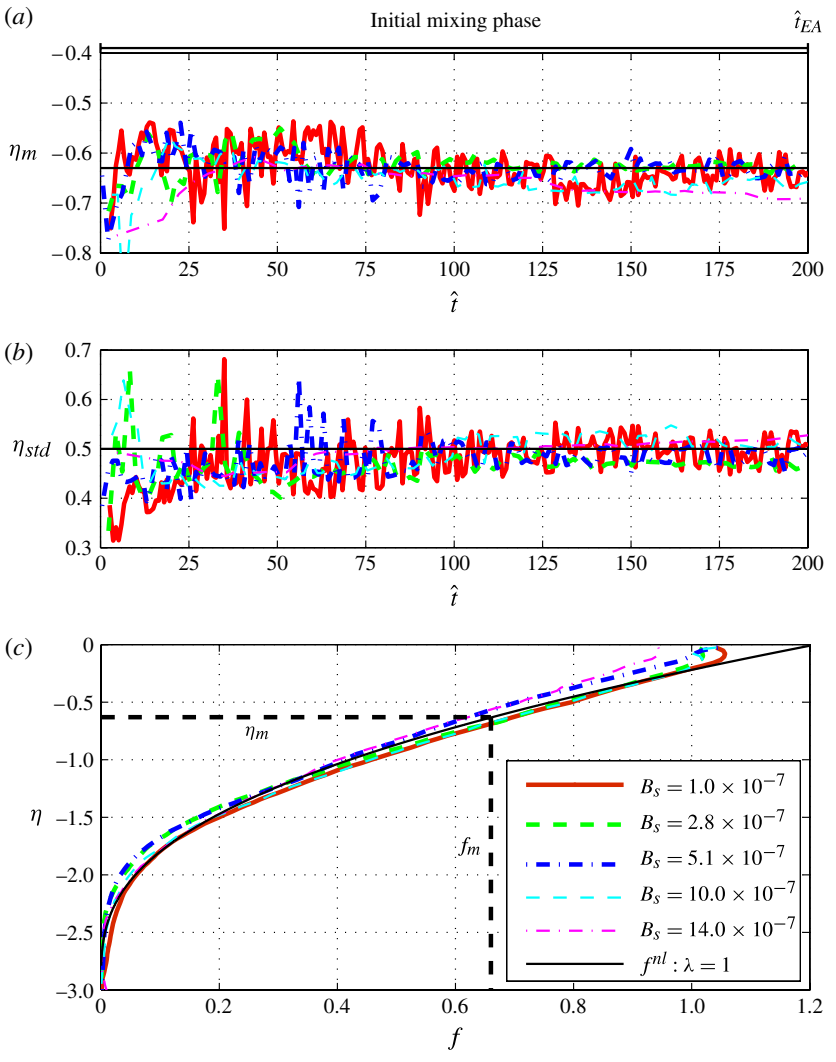

FIGURE 2. (Colour online) (*a*) The evolution of the first moment η_m as defined by (3.5); and (*b*) the evolution of the standard deviation around the first moment η_{std} as defined by (3.6) throughout the initial mixing phase $0 \leqslant \hat{t} \leqslant \hat{t}_{EA} = 200$, before the 'first front' has reached the bottom of the tank. (*c*) Profiles of non-dimensional horizontally averaged reduced gravity distribution $f(\eta)$ for the five experiments time-averaged over the initial mixing phase with: $B_s = 1.0 \times 10^{-7}$ m^4 s^{-3}; $B_s = 2.8 \times 10^{-7}$ m^4 s^{-3}; $B_s = 5.1 \times 10^{-7}$ m^4 s^{-3}; $B_s = 10.0 \times 10^{-7}$ m^4 s^{-3}; $B_s = 14.0 \times 10^{-7}$ m^4 s^{-3} and the numerical solution f^{nl} of (3.7) with boundary conditions (3.8) and (3.9) and $\lambda = 1$ (plotted with a black solid line).

in which we assume that the reduced gravity smoothly converges towards zero, near the bottom of the mixed region. Equation (3.7), subject to the conditions (3.8) and (3.9), is solved numerically by a shooting method. We guess a particular value of $f^{nl}(0)$, and then calculate (3.7) subject to (3.8) until $f^{nl} = 0$, when we check the integral constraint (3.9), iterating the whole process by updating the initial guess $f^{nl}(0)$ until this constraint is satisfied to the required precision. Furthermore, posed in this

way, we actually can calculate a one-parameter (λ) class of solutions, as both the governing equation (3.7) and the boundary condition (3.8) depend on λ.

In figure 2(*c*), we plot with a solid black line a typical solution for $f^{nl}(\eta)$ as a function of η, with $\lambda = 1$. An important observation is that $f^{nl}(\eta)$ drops from its source value (approximately 1.2) to zero at a 'front' value of $\eta_f^{nl} = -2.9$, such that $f^{nl} = 0$ for $\eta \leqslant \eta_f^{nl}$. This means that the mixed region is of finite extent, and that the gradient of f^{nl} thus drops from its source value $1/\lambda^{4/3}$ to zero at $\eta_f^{nl} = -2.9$, such that $(\partial f^{nl}/\partial\eta) = 0$ for $\eta \leqslant \eta_f^{nl}$.

From the definition of η (3.3) and the non-dimensionalization (3.1), we can now straightforwardly construct a theoretical prediction for the (non-dimensional) arrival time $\hat{t}_{PA}$,

$$\hat{t}_{PA} = \left(\frac{H}{\eta_f^{nl} d}\right)^2 = 190, \tag{3.10}$$

which is indeed in good agreement with our experimental observations and our definition of the end of the initial mixing phase $\hat{t}_{EA} = 200$, giving us further confidence in our modelling approach. Moreover, we show experimental profiles of $f(\eta)$ that are averaged over data obtained in the initial-mixing phase before the mixed region has reached the bottom of the tank, i.e. from the start of the experiment until the detectable 'first front' is $O(5d)$ from the bottom of the tank. The agreement between the experimental profiles and the model is very good, except for in the immediate vicinity of the source, i.e. at small values of η. This supports the assumption that the density distribution evolves in a self-similar fashion, and that the scalings (1.7) and (1.8) are correct.

The actual structure of the experimentally measured self-similar profile is well-predicted by our nonlinear model based around the very simple mixing length parameterization of the turbulent diffusion coefficient (1.1), in which the characteristic length scale of the turbulent eddies scale with the width of the tank d by an $O(1)$ constant λ. For our model with $\lambda = 1$, we find that $\eta_m^{nl} = -0.63$, $\eta_{std}^{nl} = 0.50$ and $f_m^{nl} = 0.66$, and we find a good agreement with experimental quantities (see table 1 and the black line in figure 2*a*). Indeed, as already noted, it is possible to identify the value of λ which minimizes the least-squares error between the experimental f-profiles and the theoretical curves obtained in the initial mixing phase. Based on this fitting procedure, we find that the 'optimal' initial mixing phase value of $\lambda_{o1} = 1.08 \pm 0.06$. In table 1, we also list the predicted values of η_m^{nl}, η_{std}^{nl} and f_m^{nl} associated with this value of λ. It is clear that the values of these quantities change by a very small amount, as does the value $\eta_f^{nl} = -3.0$ where $f^{nl} = 0$ (using $\lambda = 1.08$), thus implying that the predicted value for the arrival time reduces a little to $\hat{t}_{PA} = 178$.

4. Intermediate mixing phase

As already noted in § 2.2, experimental observations in the intermediate mixing phase suggest that the source buoyancy flux is homogeneously distributed over the height of the tank, such that the overall density gradient from top to bottom of the tank is time-independent (although as we show below the vertical structure in density gradient at any particular time is nonlinear) as the density at the top and bottom of the tank increases at the same rate. Indeed, there is a (constant) linear increase in reduced gravity at all heights with time, and so the governing turbulent diffusion equation (1.6)

	Experiments $B_s(\times 10^{-7}\ \mathrm{m}^4\ \mathrm{s}^{-3})$					Model λ	Model λ_{o1}
	1	2.8	5.1	10.0	14.0	1	1.08
η_m	-0.63 ± 0.04	-0.62 ± 0.02	-0.63 ± 0.03	-0.65 ± 0.04	-0.66 ± 0.03	-0.63	-0.67
η_{std}	0.48 ± 0.05	0.47 ± 0.03	0.48 ± 0.03	0.49 ± 0.04	0.49 ± 0.03	0.50	0.53
f_m	0.64 ± 0.06	0.70 ± 0.06	0.63 ± 0.07	0.67 ± 0.08	0.58 ± 0.05	0.66	0.63

TABLE 1. The first moment η_m as defined by (3.5), the standard deviation around the first moment η_{std} as defined by (3.6), and the non-dimensional reduced gravity $f_m = f(\eta_m)$ which are time-averaged in the initial mixing phase of the experiment. The rightmost column presents the predicted values based on our nonlinear model with $\lambda = 1$ and with the 'optimal' $\lambda_{o1} = 1.08 \pm 0.06$.

for the (dimensional) reduced gravity becomes

$$\mathscr{R} = \lambda^2 d^2 \frac{\partial}{\partial z}\left[\left(\frac{\partial \overline{g'}^{nl}}{\partial z}\right)^{3/2}\right], \tag{4.1}$$

where $\mathscr{R}$ is the constant (dimensional) rate at which the horizontally averaged reduced gravity is increasing. Under the assumption that the flux of density out of the lower opening is sufficiently small to be insignificant, the requirement that the source buoyancy flux B_s is uniformly distributed across the entire volume of the experimental tank implies that

$$\mathscr{R} = \frac{B_s}{Hd^2}. \tag{4.2}$$

Using the following non-dimensionalization (analogously to (3.1) based around the tank width d and the source buoyancy flux B_s)

$$\hat{z} = zd^{-1}; \quad \hat{g} = \overline{g'} B_s{}^{-2/3} d^{5/3}, \tag{4.3}$$

we find that the total scaled reduced gravity in the tank increases as

$$\int_{z=-H}^{0} \overline{g'}^{nl} d^2 \,\mathrm{d}z = B_s t \leftrightarrow \int_{\hat{z}=-\hat{H}}^{0} \hat{g}^{nl} \,\mathrm{d}\hat{z} = \hat{t}, \tag{4.4}$$

and that the non-dimensional reduced gravity at the bottom of the tank $z = -H$ should be

$$\overline{g'}^{nl}(-H, t) = \frac{B_s}{Hd^2}(t - t_1) \leftrightarrow \hat{g}^{nl}(-\hat{H}, \hat{t}) = \frac{\hat{t} - \hat{t}_1}{\hat{H}}, \tag{4.5}$$

where $\hat{t}_1$ is the notional time origin at which $\hat{g}(-\hat{H}, \hat{t}) = 0$. Owing to the initially non-uniform (with height) temporal increase in reduced gravity in the tank, there is an (inevitable) period of adjustment before the intermediate mixing phase model applies. The notional time $\hat{t}_1$ is therefore typically different from and larger than the actual effective arrival time $\hat{t}_{EA}$ of the 'first front' of the mixed region at the bottom of the tank.

4.1. *Scaling comparison*

In figure 3(*a*), we plot the non-dimensional reduced gravity at several heights in the tank as a function of $\hat{t} - \hat{t}_1$ for each of the experiments performed in the intermediate mixing phase. The value for $\hat{t}_1$ is chosen for each experiment to minimize the difference between the experimental data $\hat{g}(-\hat{H}, \hat{t})$ and the straight line $(\hat{t} - \hat{t}_1)/\hat{H}$ plotted with a black thick line. In this procedure, we only include experimental data with $2 < \hat{g}(-\hat{H}, \hat{t}) < 15$ to ignore the apparent initial adjustment period and to ensure that the typical reduced gravity within the tank is significantly smaller than the reduced gravity of the source. The implied value of $\hat{t}_1 = 370, 324, 374, 370$ and 380 for $B_s = 1.0, 2.8, 5.1, 10.0$ and 14.0×10^{-7} m^4 s^{-3} respectively, varies only slightly between the different experiments, and is typically larger than the value of $\hat{t}_{EA} = 200$, and we define the intermediate mixing phase by $100 \leqslant \hat{t} - \hat{t}_1 \leqslant 600$. The period of adjustment from the initial (unbounded) mixing phase to the intermediate (bounded) mixing phase is of the same order as the arrival time, since this provides the time scale required for the density profile to adjust along the whole tube.

The inset of figure 3(*a*) shows the total scaled reduced gravity plotted against non-dimensional time $\hat{t} - \hat{t}_1$. The total scaled reduced gravity increases approximately linearly as $\sim\hat{t}$, which corresponds to the constant buoyancy flux condition in non-dimensional form given by (4.4) and the black thick line plotted with a slope of one. Moreover, from figure 3(*a*), it is apparent that to a very good approximation, the reduced gravity increases homogeneously throughout the tank and linearly with time for each experiment. Unsurprisingly, there is a slight offset after the arrival of the first dense parcels of fluid at the bottom of the tank before this linear increase in the reduced gravity occurs, but eventually all experiments show the same rate of linear increase. The rate of increase, or equivalently the slope of the plotted lines for each of the heights, is also quantitatively consistent with the assumption of uniform spatial distribution of source buoyancy flux, as given by (4.5). We thus demonstrate a very good quantitative agreement with our central assumption for the intermediate mixing phase, as defined by (4.1).

4.2. *Solution of the nonlinear diffusion equation*

Using the assumption that the source buoyancy flux B_s is uniformly distributed across the entire volume of the experimental tank, it is actually possible to construct the vertical distribution of the horizontally averaged reduced gravity in the intermediate mixing phase. Substituting (4.2) into (4.1) and integrating once, we obtain

$$\frac{\partial \overline{g'}^{nl}}{\partial z} = \left(\frac{B_s}{\lambda^2 d^4}\right)^{2/3} (z/H + 1)^{2/3}, \tag{4.6}$$

where we have assumed that the natural no-flux condition at the bottom of the tank $(\partial \overline{g'}/\partial z)|_{z=-H} = 0$ is not significantly affected by the buoyancy flux out of the tank through the opening at the bottom.

Integrating again, and remembering the (equivalent) definitions for $\mathscr{R}$ (4.1)–(4.2), the predicted reduced gravity distribution at intermediate times is (using (4.3) to scale the non-dimensional form)

$$\overline{g'}^{nl} = \frac{3}{5}\left(\frac{B_s}{\lambda^2 H d^4}\right)^{2/3} (z + H)^{5/3} + \frac{B_s}{H d^2}(t - t_1), \tag{4.7}$$

$$\hat{g}^{nl} = \frac{3}{5\lambda^{4/3}\hat{H}^{2/3}} (\hat{z} + \hat{H})^{5/3} + \frac{(\hat{t} - \hat{t}_1)}{\hat{H}}, \tag{4.8}$$

where t_1 is the (notional) latest time at which $\overline{g'}(-H, t) = 0$ determined from a least-squares fitting procedure with data shown in figure 3(*a*). In figure 3(*b*), we plot against non-dimensional height the experimentally measured scaled and shifted reduced gravity profile $\hat{g} - (\hat{t} - \hat{t}_1)/\hat{H}$, averaged over the intermediate mixing phase $100 \leqslant \hat{t} - \hat{t}_1 \leqslant 600$. We also plot the theoretical prediction for the (strongly nonlinear with height) reduced gravity distribution given in (4.8) with a solid black line with the choice $\lambda = 1$, which shows a good agreement with the experimental measurements, except, once again, in the immediate vicinity of the top of the tank. Indeed, repeating a least-squares calculation to minimize the difference between the experimental profiles of $\hat{g} - (\hat{t} - \hat{t}_1)/\hat{H}$ and the theoretical model across all choices of λ, we find that the 'optimal' choice for the intermediate mixing phase experiments is $\lambda_{o2} = 1.02 \pm 0.01$.

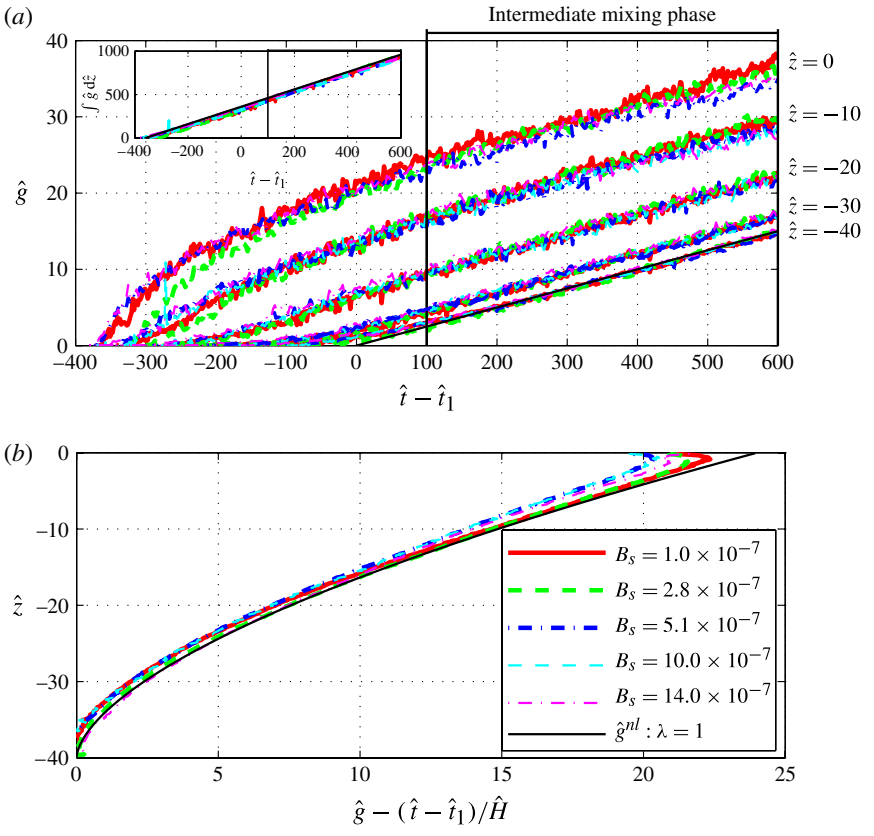

FIGURE 3. (Colour online) For the five experiments with $B_s = 1.0 \times 10^{-7}$ m^4 s^{-3}; $B_s = 2.8 \times 10^{-7}$ m^4 s^{-3}; $B_s = 5.1 \times 10^{-7}$ m^4 s^{-3}; $B_s = 10.0 \times 10^{-7}$ m^4 s^{-3}; $B_s = 14.0 \times 10^{-7}$ m^4 s^{-3} in the intermediate mixing phase $100 \leqslant \hat{t} - \hat{t}_1 \leqslant 600$: (*a*) Variation of the scaled reduced gravity at $\hat{z} = -40, -30, -20, -10$ and 0, with time $\hat{t} - \hat{t}_1$, where $\hat{t}_1$ is determined by minimizing the difference between the experimental data $\hat{g}(-\hat{H}, \hat{t})$ and the straight line $(\hat{t} - \hat{t}_1)/\hat{H}$ (plotted with a black line), the inset showing the evolution of the scaled total reduced gravity in the tank $\int \hat{g}\, d\hat{z}$ with time $\hat{t} - \hat{t}_1$, together with a black line having a slope of one, which is based on the constant buoyancy flux condition in non-dimensional form given by (4.4). (*b*) Profiles of $\hat{g} - (\hat{t} - \hat{t}_1)/\hat{H}$, averaged over the intermediate mixing phase, and the model prediction given by (4.8) with $\lambda = 1$ (plotted with a black line).

5. Linear model with constant turbulent diffusion coefficient

We have discussed a model based on Prandtl's mixing length theory, and found solutions of the nonlinear turbulent diffusion equation for both the initial and intermediate mixing phases. For the initial mixing phase, we have found that the profiles of the reduced gravity are of the self-similar form (3.4). The gradient of the reduced gravity is hence given by

$$\frac{\partial}{\partial z}\overline{g}^{nl}(z,t) = {B_s}^{2/3} d^{-8/3} \frac{\partial}{\partial \eta} f^{nl}(\eta); \quad \eta = \frac{z}{h_T} = {B_s}^{-1/6} d^{-1/3} \left(\frac{z}{t^{1/2}}\right). \tag{5.1}$$

For the intermediate mixing phase, we have derived an analytical solution for the profile of the reduced gravity (4.8). The gradient of this solution is given by

$$\frac{\partial}{\partial z}\overline{g'}^{nl}(z,t) = {B_s}^{2/3} d^{-8/3} \frac{1}{\lambda^{4/3}} \left(\frac{z}{h_T}+1\right)^{2/3}; \quad h_T = H. \tag{5.2}$$

We can thus generalize (5.1)–(5.2) into the self-similar form

$$\frac{\partial}{\partial z}\overline{g'}^{nl}(z,t) = B_s^{2/3} d^{-8/3} F^{nl}(z/h_T), \tag{5.3}$$

which implies that the gradient of the reduced gravity is given by a constant, determined by the experimental parameters B_s and d, multiplied by a shape function $F^{nl}(z/h_T)$, with z/h_T the relative position in the mixed region. The actual shape of F^{nl} is different for each mixing phase, but they have in common that $F^{nl}(0) = 1/\lambda^{4/3}$ due to the constant flux boundary condition at the top of the tank at $z = 0$ (see (3.8)).

As discussed in § 1, Barnett (1991) performed constant buoyancy flux experiments using an isolated plume source in a narrow vertical tank, and distinguished a region dominated by plume-like dynamics, a region in which the fluid is homogeneously mixed, and a region dominated by turbulent convection. For the region dominated by turbulent convection (a region corresponding to the vast majority of the flow in our experiments presented above), he applied a linear turbulent diffusion model in which the turbulent diffusion coefficient was approximated by a constant. For our constant buoyancy flux experiments, we have shown in (5.3) that the density gradient between the top and the bottom of the mixed region is independent of time for both the initial and intermediate mixing phases. The mixed region can thus be characterized by a 'typical' gradient of the reduced gravity, such that we can identify a 'typical' turbulent diffusion coefficient, which is then also independent of time and space.

Following Barnett (1991), we examine how well such a linear model with a constant turbulent diffusion coefficient predicts our experimental results. From dimensional analysis we find that a constant turbulent diffusion coefficient κ_T, and the magnitude of the associated turbulent flux of dense fluid J, should satisfy

$$\kappa_T^l = \gamma B_s^{1/3} d^{2/3} \rightarrow J^l = \gamma B_s^{1/3} d^{2/3} \frac{\partial \overline{g'}}{\partial z}, \tag{5.4}$$

with γ an $O(1)$ constant and the superscript l denoting the (assumed) underlying linear model. Indeed, the turbulent diffusion equation then takes a simple linear form

$$\frac{\partial \overline{g'}^l}{\partial t} = \gamma B_s^{1/3} d^{2/3} \frac{\partial^2 \overline{g'}^l}{\partial z^2}, \tag{5.5}$$

in which we denote the solution of this linear differential equation by $\overline{g'}^l$. This linear turbulent diffusion equation (5.5) can be solved analytically for both the initial and intermediate mixing phase.

5.1. *Initial mixing phase*

From (5.4) and the requirement of a constant buoyancy flux at $z = 0$, we find that the gradient of the reduced gravity at the top of the tank is independent of time while the total amount of buoyancy in the tank increases linearly with time. Since the mixing is believed to be self-similar, we expect that both the height of the mixed region and the reduced gravity at the top of the tank increase with the square root of time, a similar

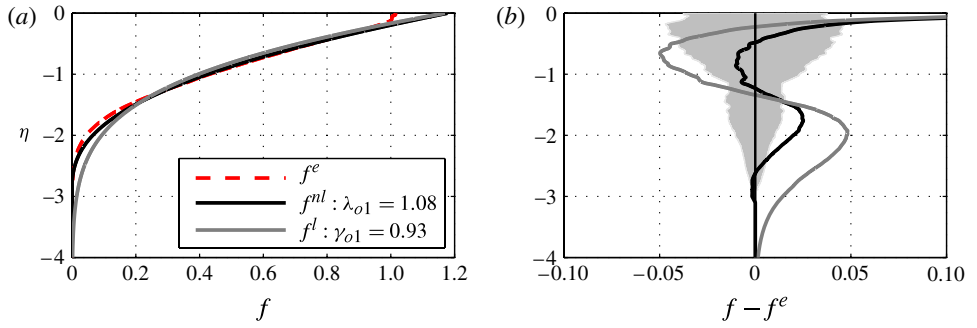

FIGURE 4. (Colour online) (*a*) Profiles against η of the theoretical solution to (3.7) f^{nl} based on a model with turbulent diffusion coefficient given by (1.5) with $\lambda_{o1} = 1.08$ (plotted with a black line), the theoretical solution (5.10) f^{l} based on a linear model with a constant turbulent diffusion coefficient given by (5.4) with $\gamma_{o1} = 0.93$ (grey line) and the average f^{e} (dashed red line) of the experimentally obtained f-profiles shown in figure 2(*c*). (*b*) Profiles against η of the differences $f^{nl} - f^{e}$ (plotted with a black line) and $f^{l} - f^{e}$ (grey line) between the average of the experimentally obtained f-profiles f^{e} and the 'optimized' theoretical solutions f^{nl} with $\lambda_{o1} = 1.08$ and f^{l} with $\gamma_{o1} = 0.93$. The grey band indicates the variation with η of the standard deviation in f^{e}.

scaling to that given by (1.7)–(1.8). Making use of the scalings (3.3), we find that the non-dimensional linear turbulent diffusion equation (5.5) is given by

$$2\gamma \frac{\partial^2 f^l}{\partial \eta^2} + \eta \frac{\partial f^l}{\partial \eta} - f^l = 0, \tag{5.6}$$

in which f^{l} denotes the solution of this linear differential equation. This equation is equivalent to

$$2\gamma \eta \frac{\partial^2}{\partial \eta^2}\left(\frac{f^l}{\eta}\right) + (4\gamma + \eta^2)\frac{\partial}{\partial \eta}\left(\frac{f^l}{\eta}\right) = 0. \tag{5.7}$$

To solve the linear non-dimensional turbulent diffusion equation (5.7), we apply two natural conditions, which are equivalent to those discussed in § 3.2. The first follows from the constant buoyancy flux located at $z = 0$, which requires the (boundary) condition (in dimensional and non-dimensional form, respectively):

$$d^2 J^l|_{z=0} = \gamma B_s^{1/3} d^{8/3} \left.\frac{\partial \overline{g'}^l}{\partial z}\right|_{z=0} = B_s \leftrightarrow \left.\frac{\partial f^l}{\partial \eta}\right|_{\eta=0} = \frac{1}{\gamma}. \tag{5.8}$$

The second (global integral) condition follows from the conservation of the total buoyancy in the entire tank of height H (with H large enough to assume $H \to \infty$)

$$d^2 \int_{-H}^{0} \overline{g'}^l \,\mathrm{d}z = B_s t \leftrightarrow \int_{-\eta_H}^{0} f^l \,\mathrm{d}\eta = 1, \tag{5.9}$$

in which we assume that the reduced gravity smoothly converges towards zero, near the bottom of the mixed region. The boundary condition (5.8) and the integral condition (5.9) are equivalent to those discussed for the nonlinear model, given by (3.8) and (3.9), respectively. The solution of (5.7) subject to the conditions (5.8) and

(5.9) is then given by

$$f^l = \sqrt{\frac{4}{\gamma\pi}}\exp(-\eta^2/4\gamma) + (\eta/\gamma)\,\mathrm{erfc}(\sqrt{\eta^2/4\gamma}). \tag{5.10}$$

Interestingly, the solution f^l converges from its source value $f^l(0) = \sqrt{4/\gamma\pi}$ towards zero for $\eta \to -\infty$, while f^{nl} drops from its source value (approximately 1.15) to zero at a 'front' value of $\eta_f^{nl} = -3.0$ (for $\lambda_{o1} = 1.08$), such that $f^{nl} = 0$ for $\eta \leqslant \eta_f^{nl}$.

To compare the experimental data with the solutions (to (3.7)) f^{nl} based on the nonlinear model and f^l (given by (5.10)) based on the linear model, we determine the average f^e of the experimental f-profiles which are shown individually in figure 2(*c*). With a least-squares fitting procedure, which minimizes the deviation between the averaged experimental profile f^e and the theoretical curve f^l, we find that the 'optimal' value for γ, as defined implicitly in (5.10), is given by $\gamma_{o1} = 0.93$. In figure 4(*a*), we plot f^e (with a red dashed line) together with the 'optimal' solutions f^l with $\gamma_{o1} = 0.93$ (grey line) and f^{nl} with $\lambda_{o1} = 1.08$ (black line; see § 3.2). In figure 4(*b*), we show the spatial variation of the difference between these 'optimized' theoretical solutions and the averaged experimentally obtained f-profiles, i.e. $(f^{nl} - f^e)$ with a black line and $(f^l - f^e)$ with a grey line. The grey band shows the spatial variation in the standard deviation for the averaged experimental profile f^e.

A normalized integral measure for the differences $(f - f^e)$ (for $f = f^{nl}$ or $f = f^l$) is given by

$$\epsilon_f = \frac{\displaystyle\int_{\eta=-\infty}^{0} \sqrt{(f-f^e)^2}\,\mathrm{d}\eta}{\displaystyle\int_{\eta=-\infty}^{0} f^e\,\mathrm{d}\eta}, \tag{5.11}$$

in which the denominator is equal to one by the definition (3.9). We find that $\epsilon_f^{nl} = 0.05$ for the nonlinear model in which the turbulent diffusion coefficient depends on the square root of the local gradient of the reduced gravity, while $\epsilon_f^l = 0.11$ for the linear model in which the turbulent diffusion coefficient is approximated by a constant.

5.2. *Intermediate mixing phase*

In the intermediate mixing phase, the mixed region has reached the bottom of the tank while the constant buoyancy flux at $z = 0$ continues. From (5.4), we thus require that the gradient of the reduced gravity at the top of the tank is independent of time. With the ongoing turbulent mixing, we believe that the buoyancy flux becomes uniformly distributed over the full height of the tank and that the density at each height increases linearly with time, similarly to the situation discussed in § 4 for the nonlinear model.

The turbulent diffusion equation (5.5) is made non-dimensional by making use of (4.3), such that

$$\frac{\partial \hat{g}^l}{\partial \hat{t}} = \gamma\frac{\partial^2 \hat{g}^l}{\partial \hat{z}^2}, \tag{5.12}$$

in which we denote the solution of this linear differential equation by $\hat{g}^l$. Owing to the assumption that the density increases linearly with time at all heights, the left-hand side of (5.12) is a constant, and so integrating (5.12) twice and applying the same

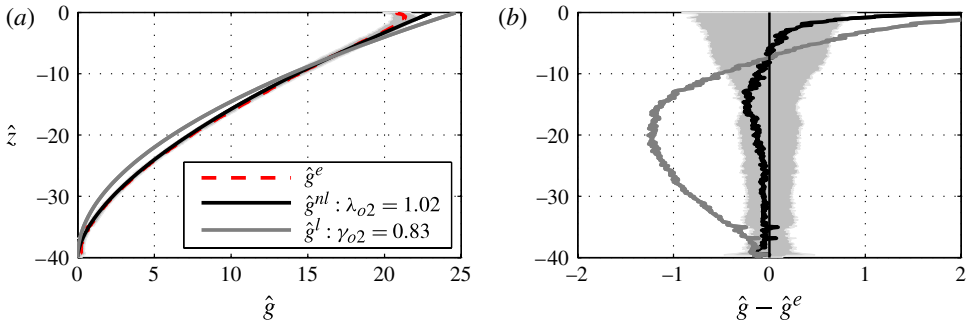

FIGURE 5. (Colour online) (*a*) Profiles against η of the theoretical solution (4.8) $\hat{g}^{nl}$ based on a model with turbulent diffusion coefficient given by (1.5) with $\lambda_{o2} = 1.02$ (plotted with a black line), the theoretical solution (5.13) $\hat{g}^l$ based on a linear model with a constant turbulent diffusion coefficient given by (5.4) with $\gamma_{o2} = 0.83$ (grey line) and the average $\hat{g}^e$ (dashed red line) of the experimentally obtained $\hat{g}$-profiles shown in figure 3(*c*). (*b*) Profiles against η of the differences $\hat{g}^{nl} - \hat{g}^e$ (plotted with a black line) and $\hat{g}^l - \hat{g}^e$ (grey line) between the average of the experimentally obtained $\hat{g}$-profiles $\hat{g}^e$ and the 'optimized' theoretical solutions $\hat{g}^{nl}$ with $\lambda_{o2} = 1.02$ and $\hat{g}^l$ with $\gamma_{o2} = 0.83$. The grey band indicates the variation with η of the standard deviation in $\hat{g}^e$.

boundary conditions as discussed in § 4.2 gives

$$\hat{g}^l = \frac{1}{2\gamma \hat{H}} (\hat{z} + \hat{H})^2 + \frac{(\hat{t} - \hat{t}_1)}{\hat{H}}. \tag{5.13}$$

To compare our experimental data with the solutions $\hat{g}^{nl}$ based on the nonlinear model, and $\hat{g}^l$ based on the linear model, we determine the average of the experimental $\hat{g}$-profiles which are shown individually in figure 3(*c*). Again, we apply a least-squares fitting procedure to minimize the deviation between the theoretical curve $\hat{g}^l$ and the averaged experimental profile $\hat{g}^e$. We find that the 'optimal' value for γ is given by $\gamma_{o2} = 0.83$. In figure 5(*a*), we plot $\hat{g}^e$ (with a dashed red line) together with the 'optimal' solutions $\hat{g}^l$ with $\gamma_{o2} = 0.83$ (grey line) and $\hat{g}^{nl}$ with $\lambda_{o2} = 1.02$ (black line; see § 4.2). In figure 5(*b*), we show the spatial variation of the difference between these 'optimized' theoretical solutions and the averaged experimentally obtained $\hat{g}$-profiles, i.e. $(\hat{g}^{nl} - \hat{g}^e)$ with a black line, and $(\hat{g}^l - \hat{g}^e)$ with a grey line. The grey band shows the spatial variation in the standard deviation for the averaged experimental profile $\hat{g}^e$. In contrast to $\hat{g}^l$, we find that the predicted $\hat{g}^{nl}$ is almost completely within the experimental error, i.e. the standard deviation in $\hat{g}^e$. A normalized integral measure for the differences $(\hat{g} - \hat{g}^e)$ (for $\hat{g} = \hat{g}^{nl}$ or $\hat{g} = \hat{g}^l$) is given by

$$\epsilon_g = \frac{\displaystyle\int_{\hat{z}=-\hat{H}}^{0} \sqrt{(\hat{g} - \hat{g}^e)^2}\, \mathrm{d}\hat{z}}{\displaystyle\int_{\hat{z}=-\hat{H}}^{0} \hat{g}^e\, \mathrm{d}\hat{z}}, \tag{5.14}$$

in which the denominator is found to be equal to 345. We find that $\epsilon_g^{nl} = 0.017$ for the nonlinear model in which the turbulent diffusion coefficient depends on the square root of the local gradient of the reduced gravity, while $\epsilon_g^l = 0.097$ for the linear model in which the turbulent diffusion coefficient is approximated by a constant.

For both the initial and intermediate mixing phase, we find that the two 'optimized' models overpredict the experimental data near the top of the mixed region, i.e. $-0.3 \lesssim \eta < 0$ for the initial mixing phase and $-5 \lesssim \hat{z} < 0$ for the intermediate mixing phase, as is apparent in figures 4(*a*) and 5(*b*). We believe that this mismatch is caused by the local source dynamics, where the characteristic scales of the turbulent flow still grow towards the full extent of the tank. A more detailed discussion of this topic is given in the next section.

6. Assumption validity

There are two important assumptions implicit in our nonlinear model of the experiments. First, we assume that the buoyancy-driven turbulence extends the whole distance across the tank, and thus has a single characteristic length scale (d). As is apparent from the structure of the reduced gravity profiles shown in figures 4(*b*) and 5(*b*), there is clearly different behaviour in the immediate vicinity of the source, i.e. over length scales $z \sim O(d)$. Although we attempt to spread the source of dense fluid across the whole cross-sectional area of the tank through the use of a fine mesh, near the source there is inevitably a tendency for a 'plume' of dense fluid to descend. This descending plume entrains and mixes with the fluid in the tank, until the descending fluid becomes affected by the tank walls, thus leading to the turbulent flow extending across the whole tank.

A conservative estimate for the width of this plume at a distance z from the source can be constructed from the assumption that the plume behaves like the classical similarity solution first considered by Morton *et al.* (1956) and so the half-width $b(z)$ depends linearly on z like

$$b \simeq \frac{6\alpha z}{5}, \quad \alpha \simeq 0.1, \tag{6.1}$$

where α is the so-called 'entrainment constant'. Therefore, we expect the plume to be strongly affected by the walls of the tank at the furthest by $b \simeq d/2$, i.e.

$$z \sim \frac{50}{12} d \sim 4d, \tag{6.2}$$

and so we expect the turbulence to extend across the entire tank when $z > 5d$, which is entirely consistent with the region of adjustment shown in figures 2(*c*) and 3(*b*). This is actually also consistent with the results of the deliberately localized plume experiments performed by Barnett (1991), suggesting that our source is still somewhat plume-like in its behaviour, or that the flow itself organizes into a 'plume' at least very close to the top of the tank.

The second assumption is that the source of buoyancy has negligible mass flux; this corresponds to the limit in which B_s is finite, $g_s' \to \infty$ and $Q_s \to 0$. However, in the actual experiments, both Q_s and g_s are non-zero and finite. In the initial mixing phase, when the mixed region is deepening, the reduced gravity of the source fluid is much larger than the reduced gravity at the top of the tank, provided that $g_s' \gg B_s^{5/6} d^{-7/3} t^{1/2}$. The reduced gravity at the top of the tank increases with time, and so in the initial mixing phase the reduced gravity reaches its largest value when the mixed region finally extends over the entire height of the tank, i.e. when $t \simeq t_{PA} = (H/\eta_f)^2 B_s^{-1/3} d^{-2/3}$, using (3.10) and (3.1). It is important to remember that $\eta_f \simeq -3$ for $\lambda = 1$ is the value of the similarity variable η at the front of the mixed region during the initial mixing phase (as discussed in more detail in § 3.2). Therefore, to apply our nonlinear model to

the initial mixing phase, we require that $g'_s \gg (H/|\eta_f|)B_s^{2/3}d^{-8/3}$, equivalent to

$$\phi = \frac{B_s^{1/3}d^{5/3}}{Q_s} \gg \frac{H}{|\eta_f|d}. \tag{6.3}$$

For our experiments $H/(|\eta_f|d) \simeq 13$, while $55 \leqslant \phi \leqslant 315$, and so this condition is satisfied for the initial mixing phase of the experiments.

A similar requirement can be derived for the intermediate mixing phase. We find that the source reduced gravity is much larger than the reduced gravity at the top of the tank when $g'_s \gg g'(0)$, with $g'(0)$ given by (4.7). At the end of the intermediate mixing phase, we find that the reduced gravity at the top of the tank is 45 % of g'_s for the highest buoyancy flux experiments and 7 % of g'_s for the lowest buoyancy flux experiments. Eventually, the reduced gravity within the tank will converge exponentially, in a final 'well-mixed' phase, to the source reduced gravity on a time scale given by the 'replacement time scale' t_r defined as

$$t_r = \frac{Hd^2}{Q_s}, \tag{6.4}$$

i.e. the time to fill the tank in the absence of mixing by the inflowing volume flux. (See Caulfield & Woods (2002) for a detailed discussion of the long-time effect of finite source volume fluxes on filling box flows.) For our experiments, the replacement time scale is $t_r \simeq 6 \times 10^3$ s for the highest, and $t_r \simeq 7 \times 10^4$ s for the lowest buoyancy flux experiments. The ultimate duration of our experiments range between 1.5×10^3 and 2.5×10^3 s for the highest and lowest buoyancy flux experiments, respectively. We conclude that the assumption that the flow is in the intermediate mixing phase, and not in the final well-mixed phase is likely to be valid throughout the experiments' duration for the flows with smaller source buoyancy flux, but is close to being violated by the flows with larger source buoyancy flux, although it typically appears to take approximately $5t_r$ for the flow to adjust fully to its well-mixed state, as discussed in Caulfield & Woods (2002).

Another aspect of the flow which is associated with the finite source volume flux is that there is a net flow through the tank due to the outflow opening at the bottom of the tank. In the intermediate mixing phase, when the mixed region has reached the bottom, there is thus a non-zero buoyancy flux leaving the tank through the outflow opening. The net buoyancy flux in the tank is therefore given by the constant buoyancy flux at the top minus the buoyancy flux leaving the tank at the bottom, i.e.

$$B_{ns} = [g'_s - g'(-H)]Q_s. \tag{6.5}$$

Our modelling assumption of a net constant buoyancy flux is valid provided that $B_{ns} \approx B_s$, or equivalently $g'(-H) \ll g'_s$. At the end of the period we are considering experimentally the intermediate mixing phase, we find that the net buoyancy flux is $B_{ns} \simeq 0.82B_s$ for the highest buoyancy flux experiments and $B_{ns} \simeq 0.97B_s$ for the lowest buoyancy flux experiments. The discrepancy from a constant net buoyancy flux of B_s is non-trivial, especially for the highest buoyancy flux experiments. This is entirely consistent with the fact that the duration of the experiment is smaller, but of the same order as the replacement time scale t_r as defined in (6.4). However, a least-squares fitting procedure that minimizes the error between a straight line and the total scaled reduced gravity, as shown in the inset of figure 3(*a*), reveals that the average of the net buoyancy flux throughout the intermediate mixing phase of the highest buoyancy flux experiments flux is still $\overline{B}_{ns} = 0.96B_s$. We hence believe

that the modelling assumption of a constant net buoyancy flux B_s is reasonably valid throughout the intermediate mixing phase, even for the highest buoyancy flux experiments.

Finally, the net flow through the tank also has implications for the flow dynamics. The net flow has a characteristic velocity $v_n = Q_s/d^2$, and we assume that this velocity is much smaller in magnitude than the characteristic buoyancy-driven velocity scale in both mixing phases, i.e.

$$v_n \ll v_b = \left(\frac{B_s}{d}\right)^{1/3} \rightarrow Q_s \ll B_s^{1/3} d^{5/3} \leftrightarrow \phi \gg 1. \tag{6.6}$$

This condition is once again less stringent than that given by (6.3), and so during our experiments, we believe that our underlying assumptions are adequately valid for our models to be applicable.

7. Conclusion and discussion

In this paper, we consider the turbulent mixing which results from a constant buoyancy flux B_s at the top of a long narrow vertical tank with square cross-section $d \times d$ and height $H = 40d$ (where $d = 5$ cm). In our experiments, the source buoyancy flux corresponds to the injection of a small constant volume flux of dense fluid. The injected fluid vigorously mixes with the less dense fluid that initially occupies the tank, such that a dense mixed region of turbulent fluid propagates downwards. We discuss both the initial mixing phase before and the intermediate mixing phase after the mixed region has reached the bottom of the tank. For both mixing phases, we restrict ourselves to the situation where the typical density in the tank is still significantly smaller than the source density. We show that the turbulent vertical transport of density may be modelled as a turbulent diffusive process with the turbulent diffusion coefficient and the magnitude of the local turbulent flux given by $\kappa_T^{nl} = \lambda^2 d^2 \left(\partial \overline{g'}/\partial z\right)^{1/2}$ and $J^{nl} = \lambda^2 d^2 \left(\partial \overline{g'}/\partial z\right)^{3/2}$, respectively. We refer to this as a nonlinear model, as it naturally leads to a nonlinear diffusion equation for the reduced gravity. The $O(1)$ constant λ relates the width of the tank to the characteristic mixing length of the turbulent eddies.

Physically, this dependence implies that mixing properties are dominated by the present, local values of the density gradient. Using this simple modelling framework in the case of a constant buoyancy flux, we find that the overall density gradient between the top and bottom of the mixed region is independent of time. From a physical point of view, this can be explained by counterflowing eddies which are generated by the gradient of buoyancy. If the gradient of buoyancy weakens, the flow will slow down and the gradient will build up, and if it gets too strong the counterflow will speed up to weaken the gradient.

In the initial mixing phase, we show that the height of the mixed region h, and the reduced gravity at the top of the tank $\overline{g'}(0)$ both increase like $t^{1/2}$. In particular, we find that the first moment of the density distribution grows as $z_m = \eta_m h_T \approx -0.63 {B_s}^{1/6} d^{1/3} t^{1/2}$, and that the corresponding moment of the reduced gravity increases as $g'_m = f_m \overline{g'}_T(0) \approx 0.66 {B_s}^{5/6} d^{-7/3} t^{1/2}$. Our model also yields a self-similar solution for the structure of the reduced gravity profile within the deepening mixed region, which we calculate numerically and successfully compare with experimental measurements based on a dye attenuation technique. We find that the effective arrival time t_{EA} (estimated to be somewhat less than the experimentally

measured arrival time of the detectable 'first front' t_{DA}) of this mixed region at the bottom of the tank is also well-predicted by our model.

In the intermediate mixing phase, which onsets after a certain adjustment time after the end of the initial mixing phase, the height of the mixed region is not able to grow further while the buoyancy flux, and hence the overall density gradient between the top and the bottom of the tank, is still constant. This suggests that the buoyancy flux is uniformly distributed across the entire height of the tank. We show that the assumption that the density increases approximately linearly with time at all heights is valid during this intermediate mixing phase. This leads to an analytical description of the density profile, which is nonlinear (actually cubic) with height and shows good agreement with experimental results.

In this paper, we use a nonlinear model for the turbulent diffusion coefficient that was successfully applied by numerous previous studies on buoyancy-driven mixing in narrow vertical tanks, see Holmes *et al.* (1991), Baird *et al.* (1992), Zukoski (1995) and Dalziel *et al.* (2008). For our constant buoyancy flux experiments, we show that the mixed region is characterized by a 'typical' density gradient. This means that we can identify a 'typical' turbulent diffusion coefficient that is independent of both space and time. Therefore, following Barnett (1991), we test the predictions based on a model in which the turbulent diffusion coefficient is approximated by a constant. This inherently linear model assumes that the turbulent diffusion coefficient and the magnitude of the local turbulent flux are given by $\kappa_T^l = \gamma B_s^{1/3} d^{2/3}$ and $J^l = \gamma B_s^{1/3} d^{2/3} (\partial \overline{g'}/\partial z)$, respectively, with γ an $O(1)$ constant. Interestingly, for the initial mixing phase, the scalings for the depth of the mixed region and the reduced gravity at the top of the mixed region are the same for both the linear and the nonlinear model.

For both mixing phases, we show that the 'optimized' solutions (in terms of λ and γ) based on the nonlinear and linear model predict the experimental data quite well. For the initial mixing phase, we find that the normalized integral measure for the difference between theory and experiment (as defined in (5.11)) is $\epsilon_f^{nl} = 0.05$ (with the 'optimal' choice of $\lambda_{o1} = 1.08$) and $\epsilon_f^l = 0.11$ (with the 'optimal' choice of $\gamma_{o1} = 0.93$) for the nonlinear model and linear model, respectively. For the intermediate mixing phase, we find that the equivalent normalized integral measure for the difference between theory and experiment (as defined in (5.14)) is $\epsilon_g^{nl} = 0.017$ (with the 'optimal' choice of $\lambda_{o2} = 1.02$) and $\epsilon_g^l = 0.097$ (with the 'optimal' choice of $\gamma_{o2} = 0.83$) for the nonlinear model and the linear model, respectively.

The particular values of these normalized integral measures of difference imply that the experimental data obtained in the intermediate mixing phase is typically better predicted by the theoretical solutions, compared with that for the experimental data obtained in the initial mixing phase. This is most likely caused by a longer time-averaging interval and the flow being more fully developed during the intermediate mixing phase. Furthermore, both the nonlinear and linear model do not include the local source dynamics, where the characteristic scales of the turbulent flow still grow towards the full width of the tank. This means that deviations between the experimental data and the theoretical solutions are to be expected, in particular during the early stage of the initial mixing phase, where the mixed region is still relatively shallow and therefore more affected by the local source dynamics.

The 'optimized' solutions based on the nonlinear model are found to have smaller differences with the experimental data than the 'optimized' solutions based on the linear model. This is especially the case for the intermediate mixing phase, where

the normalized integral measure for the difference ϵ_g^{nl} ($\lambda_{o2} = 1.02$) is almost six times smaller than the corresponding value for the linear model. Furthermore, the difference between the 'optimized' solution $\hat{g}^{nl}$ and the averaged experimental profile $\hat{g}^e$, i.e. $(\hat{g}^{nl} - \hat{g}^e)$, is almost completely within the experimental error in $\hat{g}^e$, as can be seen in figure 5(*b*).

We find that the 'optimal' values for λ are given by $\lambda_{o1} = 1.08$ for the initial mixing phase and $\lambda_{o2} = 1.02$ for the intermediate mixing phase. This is consistent with Dalziel *et al.* (2008) who assumed $\lambda = 1$ in modelling Rayleigh–Taylor experiments in a similar tank with $d = 5$ cm. Furthermore, we find that our optimal value is within the range described by Baird *et al.* (1992) who performed finite source release experiments with water-salt solutions and found that $\lambda = 1.42$ for $d = 1.48$ cm, $\lambda = 1.26$ for $d = 1.91$ cm and $\lambda = 0.95$ for $d = 2.63$ cm. Different values of d can be interpreted as corresponding to experiments with different characteristic Reynolds numbers. Experiments were also performed with fluids which have a viscosity nine times that of water, and their reported values of λ decrease towards one with decreasing viscosity. Therefore, it can be deduced that the turbulent mixing length decreases towards the width of the tank (i.e. $\lambda \to 1^+$) with increasing Reynolds number. This is consistent with our high Reynolds number experiments where we find optimal values of λ very close to one. Furthermore, in § 6, we consider the range of validity of the key underlying assumptions of our nonlinear model, and thus explain some observed differences between our experimental measurements and theoretical predictions.

Finally, it is interesting to consider briefly a real-world application, and so we apply our initial mixing phase model as a simple model for a mineshaft accident. In the event of a methane leakage ($\rho_s = 0.7$ kg m^{-3} and $Q_s = 10^{-3}$ m^3 s^{-1}) at the bottom of a vertical mineshaft filled with air ($\rho_0 = 1.2$ kg m^{-3}) and square cross-section with width $d = 1$ m, we can estimate the height of the first moment h_m of the vertical methane distribution. Based on our model, we find that $h_m \approx 0.63 {B_s}^{1/6} d^{1/3} t^{1/2}$ with $g'_m \approx -0.66 {B_s}^{5/6} d^{-7/3} t^{1/2}$, or in terms of the volume concentration $c_m = (\rho_0 - \rho)/(\rho_0 - \rho_s) \approx 0.66\, {g'_s}^{-1} {B_s}^{5/6} d^{-7/3} t^{1/2}$. With $g'_s = g(\rho_s - \rho_0)/\rho_0 = 4.1$ ms^{-2} and $B_s = g'_s Q_s = 4.1 \times 10^{-3}$ m^4 s^{-3}, we find that the first moment with volume concentration 6.6 % reaches 10 m after almost 26.5 minutes and that the first moment with volume concentration 19.6 % reaches 30 m after almost 4 hours.

Here, we have demonstrated the power of our modelling approach to describe the turbulent mixing driven by a constant source of buoyancy flux at the top of a long narrow tank originally filled with quiescent fluid of a different density. This demonstration naturally suggests some generalizations of interest, particularly concerning the properties of the fluid within the tank initially. Counterflow within the tank would be expected to arrest the descent of the dense layer, thus leading to a steady state, while if the fluid was initially stratified within the tank, the penetrative entrainment by the descending layer would presumably be modified in a non-trivial way. We intend to report on the results of our investigation of these and related phenomena in due course, in particular the connections between this flow and the various 'filling box' flows of isolated plumes in containers.

Acknowledgements

This work has been funded through the BP Institute and EPSRC. We gratefully acknowledge the technical assistance of A. Pluck, and the constructive comments of three anonymous referees.

REFERENCES

AHLERS, G., GROSSMANN, S. & LOHSE, D. 2009 Heat transfer and large scale dynamics in turbulent Rayleigh–Bénard convection. *Rev. Mod. Phys.* **81**, 503–537.

BAINES, W. D. & TURNER, J. S. 1969 Turbulent buoyant convection from a source in a confined region. *J. Fluid Mech.* **37**, 51–80.

BAIRD, M. H. I., ARAVAMUDAN, K., RAO, N. V. R., CHADAM, J. & PEIRCE, A. P. 1992 Unsteady axial mixing by natural convection in a vertical column. *AIChE J.* **38**, 1825–1834.

BARNETT, S. 1991 The dynamics of buoyant releases in confined spaces. PhD thesis, DAMTP University of Cambridge.

CAULFIELD, C. P. & WOODS, A. W. 2002 The mixing in a room by a localized finite-mass-flux source of buoyancy. *J. Fluid Mech.* **471**, 33–50.

CENEDESE, C. & DALZIEL, S. B. 1998 Concentration and depth fields determined by the light transmitted through a dyed solution. In *Proceedings of the 8th International Symposium on Flow Visualization* (ed. G. M. Carlomango & I. Grant), ISBN 0953399109, Paper 061.

DALZIEL, S. B., PATTERSON, M. D., CAULFIELD, C. P. & COOMARASWAMY, I. A. 2008 Mixing efficiency in high-aspect-ratio Rayleigh–Taylor experiments. *Phys. Fluids* **20**, 065106.

DEBACQ, M., FANGUET, V., HULIN, J. P., SALIN, D. & PERRIN, B. 2001 Self-similar concentration profiles in buoyant mixing of miscible fluids in a vertical tube. *Phys. Fluids* **13**, 3097–3100.

DIMONTE, G., YOUNGS, D. L., DIMITS, A., WEBER, S., MARINAK, M., WUNSCH, S., GARASI, C., ROBINSON, A., ANDREWS, M. J., RAMAPRABHU, P., CALDER, A. C., FRYXELL, B., BIELLO, J., DURSI, L., MACNEICE, P., OLSON, K., RICKER, P., ROSNER, R., TIMMES, F., TUFO, H., YOUNG, Y. N. & ZINGALE, M. 2004 A comparative study of the turbulent Rayleigh–Taylor instability using high-resolution three-dimensional numerical simulations: The Alpha-Group Collaboration. *Phys. Fluids* **16**, 1668–1693.

HOLMES, T. L., KARR, A. E. & BAIRD, M. H. I. 1991 Effect of unfavourable continuous phase density gradient on axial mixing. *AIChE J.* **37**, 360–366.

KARMIS, M. 2001 *Mine Health and Safety Management*. SME.

LIDE, D. R. (Ed.) 2001 *CRC Handbook of Chemistry and Physics*, 82nd edn. CRC.

MORTON, B. R., TAYLOR, G. I. & TURNER, J. S. 1956 Turbulent gravitational convection from maintained and instantaneous sources. *R. Soc. Lond. Proc. Ser.* A **234**, 1–23.

RYAN, M. P. 1994 *Magmatic Systems (International Geophysics Series)*. Academic.

THAKORE, S. B. & BHATT, B. I. 2007 *Introduction to Process Engineering and Design*. Tata McGraw-Hill.

WEISS, S. & AHLERS, G. 2011 Turbulent Rayleigh–Bernard convection in a cylindrical container with aspect ratio $\gamma = 0.50$ and Prandtl number $Pr = 4.38$. *J. Fluid Mech.* **676**, 5–40.

WOODS, A. W. 2010 Turbulent plumes in nature. *Annu. Rev. Fluid Mech.* **42**, 391–412.

ZUKOSKI, E. E. 1995 Review of flows driven by natural convection in adiabatic shafts. *Tech. Rep.* NIST-GCR-95-679. U.S. Department of Commerce, National Institute of Standard and Technology, Building and Fire Research Laboratory.